Campbell, L.P. *et al.* 2015. Climate change influences on global distributions of dengue and chikungunya virus vectors. *Phil. Trans. R. Soc. B.* **370** doi: 10.1098/rstb.2014.0135

Supplementary Materials

Figure S1. Summary of modeled potential distributional patterns of *Aedes aegypti* under present-day conditions based on analysis of 6 principal components.

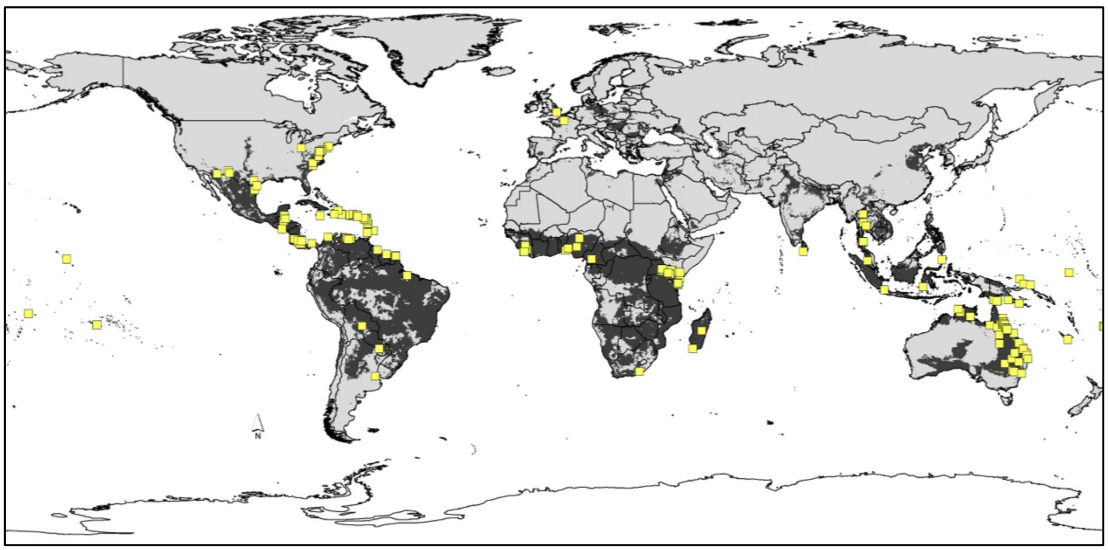

Figure S2. Summary of modeled potential distributional patterns of *Aedes albopictus* under present-day conditions based on analysis of 6 principal components.

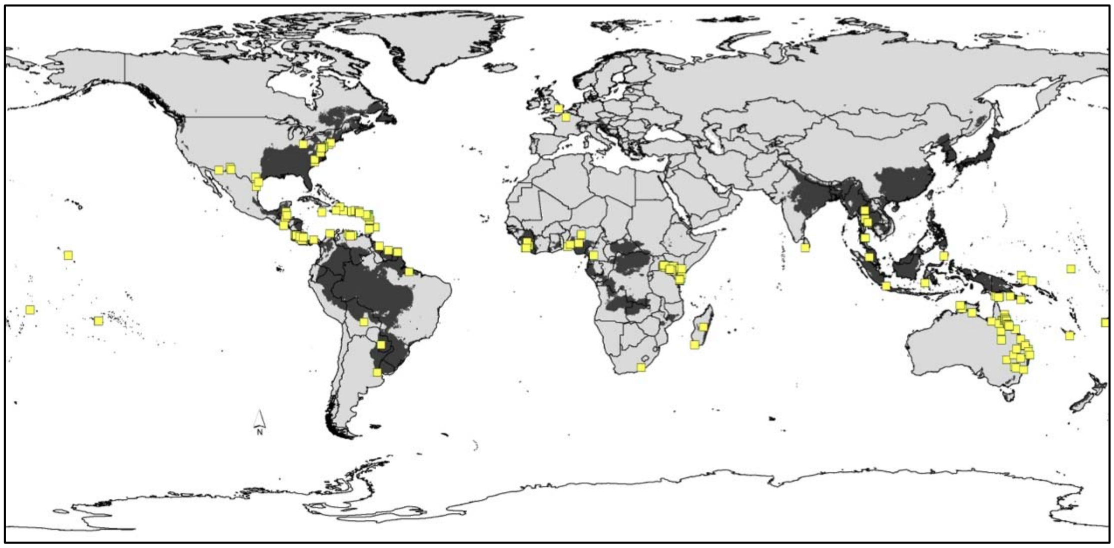

Figure S3. Summary of modeled potential distributional patterns of *Aedes aegypti* under future conditions (B1) based on analysis of 8 principal components. Confidence in present-day and future distributional potential is based on agreement among 5 climate models (Table 1): present-day distributional areas are shown in blue, with model agreement shown as shades of blue (light blue = low, dark blue = high model agreement); future distributional potential is shown as shades of orange (light orange = low, dark orange = high model agreement).

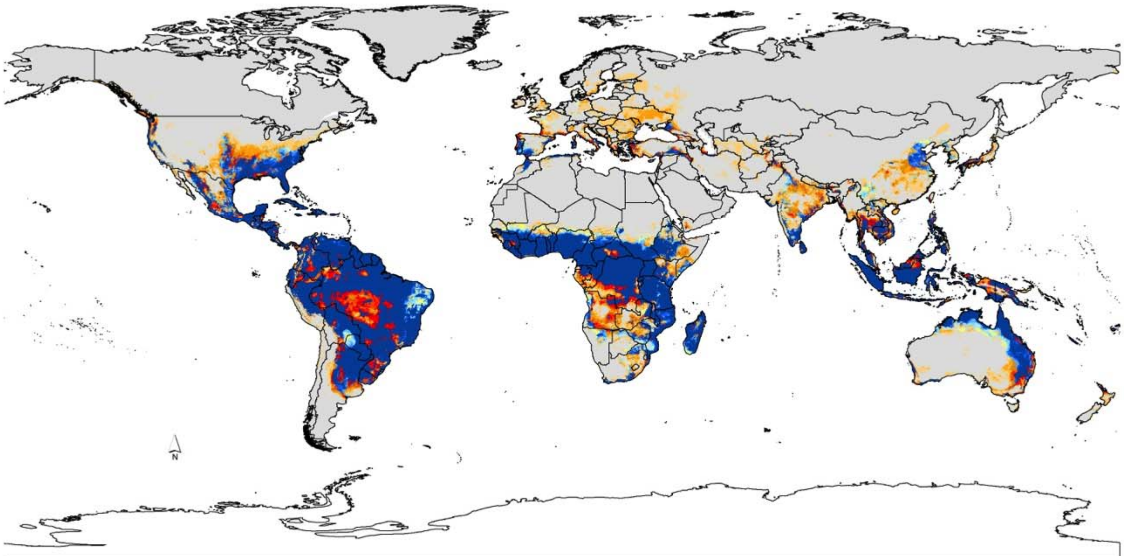

Figure S4. Summary of modeled potential distributional patterns of *Aedes albopictus* under future conditions (B1) based on analysis of 8 principal components. Confidence in present-day and future distributional potential is based on agreement among 5 climate models (Table 1): present-day distributional areas are shown in blue, with model agreement shown as shades of blue (light blue = low, dark blue = high model agreement); future distributional potential is shown as shades of orange (light orange = low, dark orange = high model agreement).

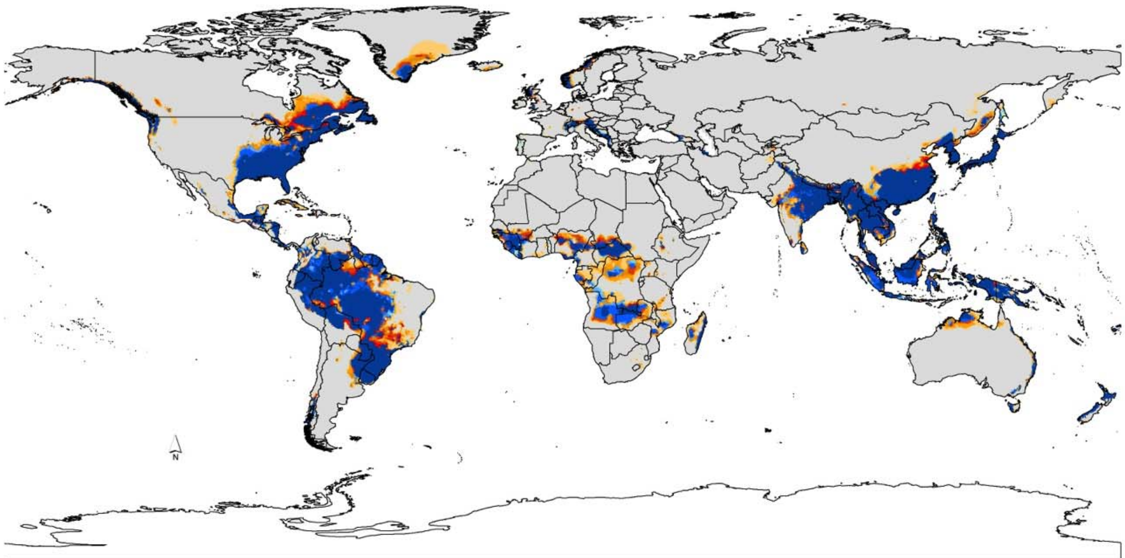

Figure S5. Summary of modeled potential distributional patterns of *Aedes aegypti* under future conditions (A2) based on analysis of 8 principal components. Confidence in present-day and future distributional potential is based on agreement among 6 climate models (Table 1): present-day distributional areas are shown in blue, with model agreement shown as shades of blue (light blue = low, dark blue = high model agreement); future distributional potential is shown as shades of orange (light orange = low, dark orange = high model agreement).

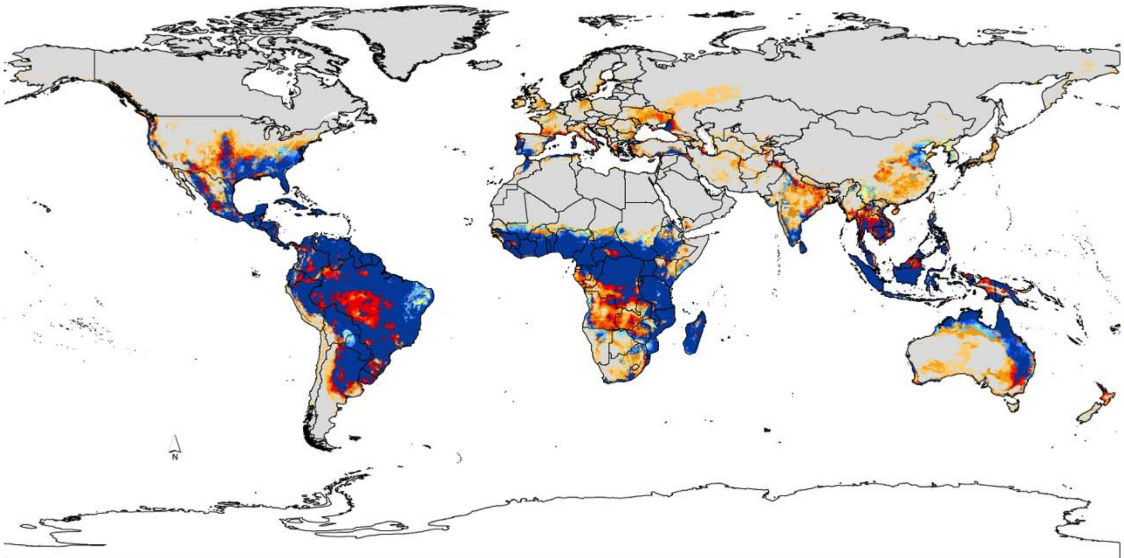

Figure S6. Summary of modeled potential distributional patterns of *Aedes albopictus* under future conditions (A2) based on analysis of 8 principal components. Confidence in present-day and future distributional potential is based on agreement among 6 climate models (Table 1): present-day distributional areas are shown in blue, with model agreement shown as shades of blue (light blue = low, dark blue = high model agreement); future distributional potential is shown as shades of orange (light orange = low, dark orange = high model agreement).

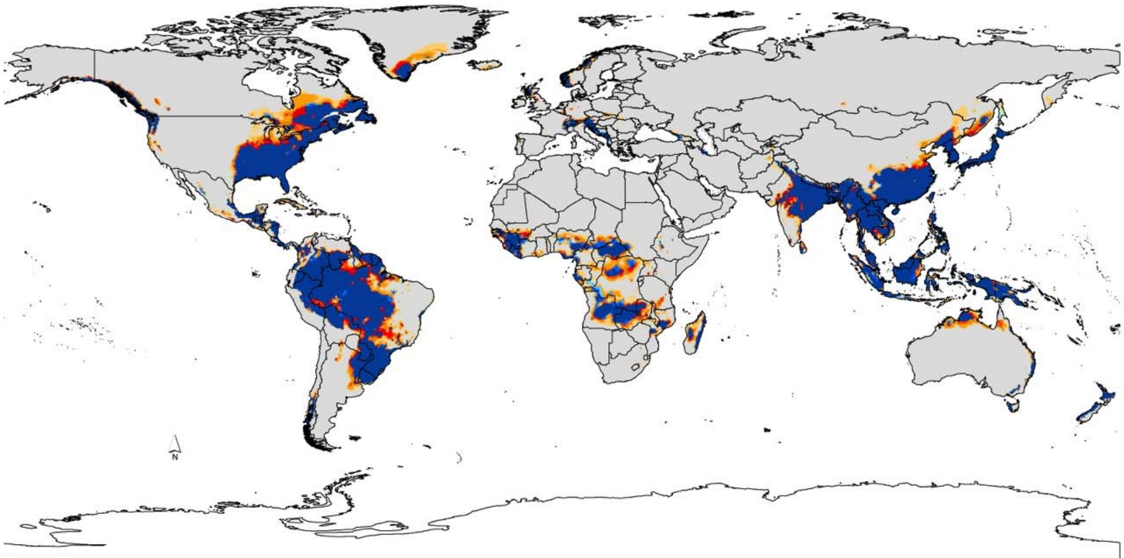

Figure S7. Summary of modeled potential distributional patterns of *Aedes aegypti* under future conditions (A1B) based on analysis of 6 principal components. Confidence in present-day and future distributional potential is based on agreement among 6 climate models (Table 1): present-day distributional areas are shown in blue, with model agreement shown as shades of blue (light blue = low, dark blue = high model agreement); future distributional potential is shown as shades of orange (light orange = low, dark orange = high model agreement).

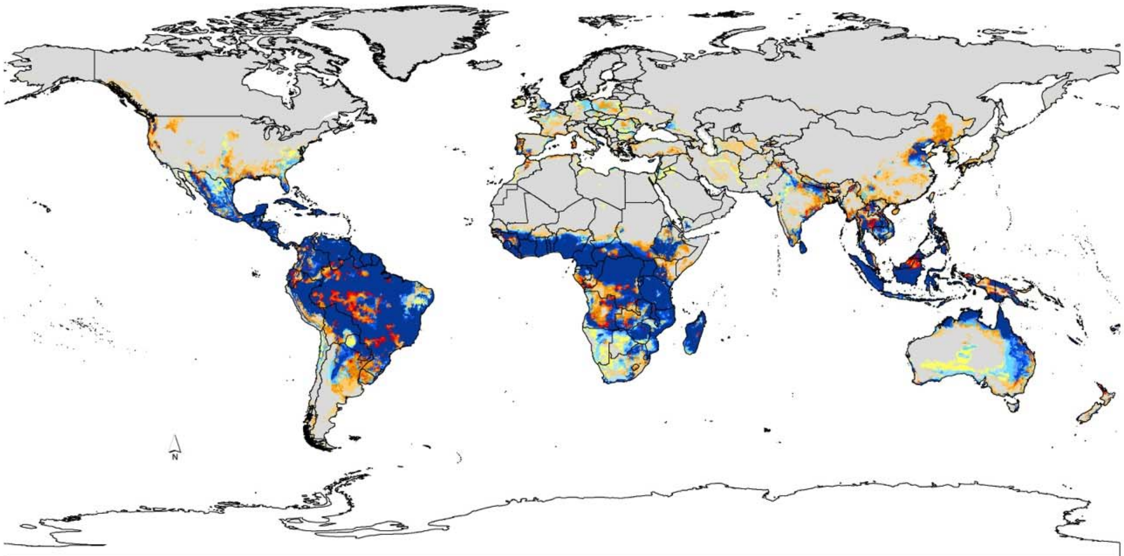

Figure S8. Summary of modeled potential distributional patterns of *Aedes albopictus* under future conditions (A1B) based on analysis of 6 principal components. Confidence in present-day and future distributional potential is based on agreement among 6 climate models (Table 1): present-day distributional areas are shown in blue, with model agreement shown as shades of blue (light blue = low, dark blue = high model agreement); future distributional potential is shown as shades of orange (light orange = low, dark orange = high model agreement).

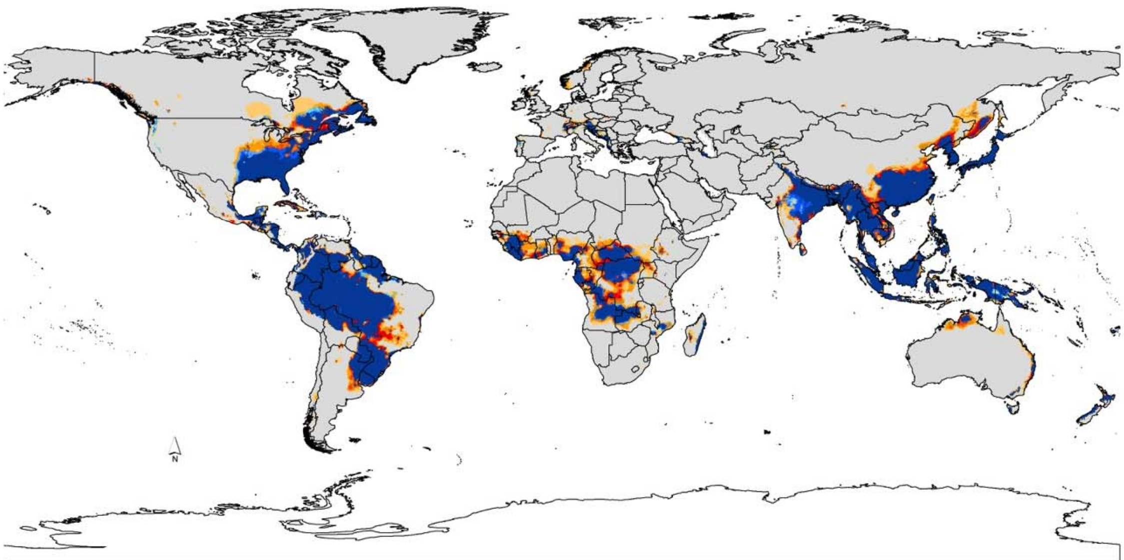

Figure S9. Summary of modeled potential distributional patterns of *Aedes aegypti* under future conditions (B1) based on analysis of 6 principal components. Confidence in present-day and future distributional potential is based on agreement among 5 climate models (Table 1): present-day distributional areas are shown in blue, with model agreement shown as shades of blue (light blue = low, dark blue = high model agreement); future distributional potential is shown as shades of orange (light orange = low, dark orange = high model agreement).

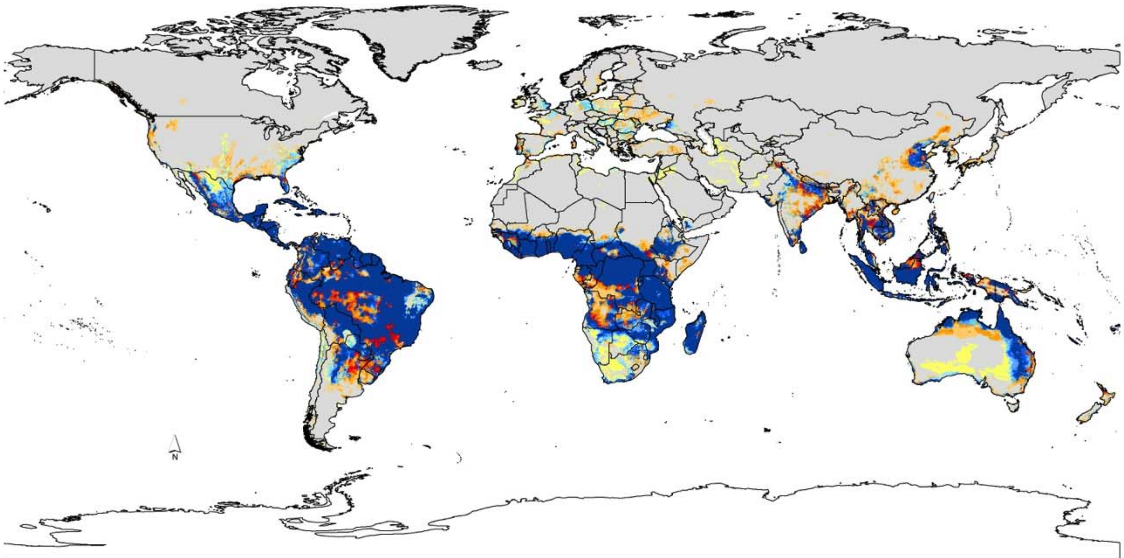

Figure S10. Summary of modeled potential distributional patterns of *Aedes albopictus* under future conditions (B1) based on analysis of 6 principal components. Confidence in present-day and future distributional potential is based on agreement among 5 climate models (Table 1): present-day distributional areas are shown in blue, with model agreement shown as shades of blue (light blue = low, dark blue = high model agreement); future distributional potential is shown as shades of orange (light orange = low, dark orange = high model agreement).

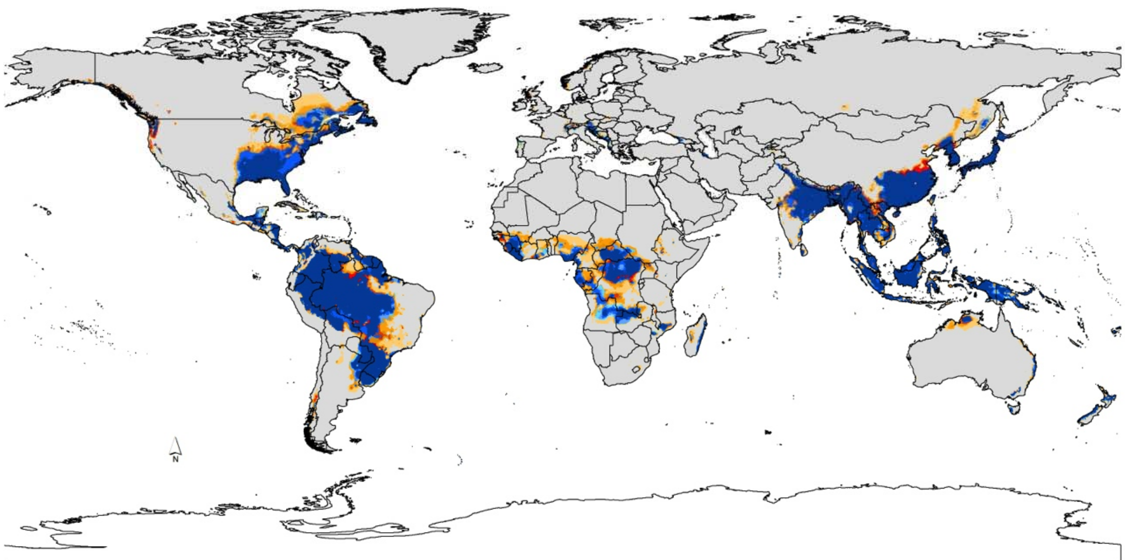

Figure S11. Summary of modeled potential distributional patterns of *Aedes aegypti* under future conditions (A2) based on analysis of 6 principal components. Confidence in present-day and future distributional potential is based on agreement among 6 climate models (Table 1): present-day distributional areas are shown in blue, with model agreement shown as shades of blue (light blue = low, dark blue = high model agreement); future distributional potential is shown as shades of orange (light orange = low, dark orange = high model agreement).

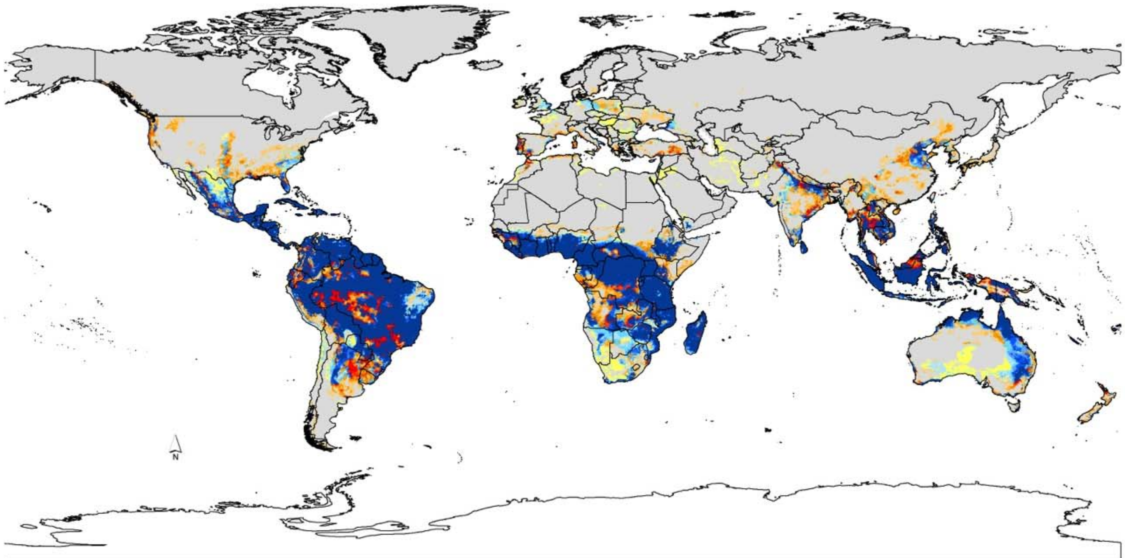

Figure S12. Summary of modeled potential distributional patterns of *Aedes albopictus* under future conditions (A2) based on analysis of 6 principal components. Confidence in present-day and future distributional potential is based on agreement among 6 climate models (Table 1): present-day distributional areas are shown in blue, with model agreement shown as shades of blue (light blue = low, dark blue = high model agreement); future distributional potential is shown as shades of orange (light orange = low, dark orange = high model agreement).

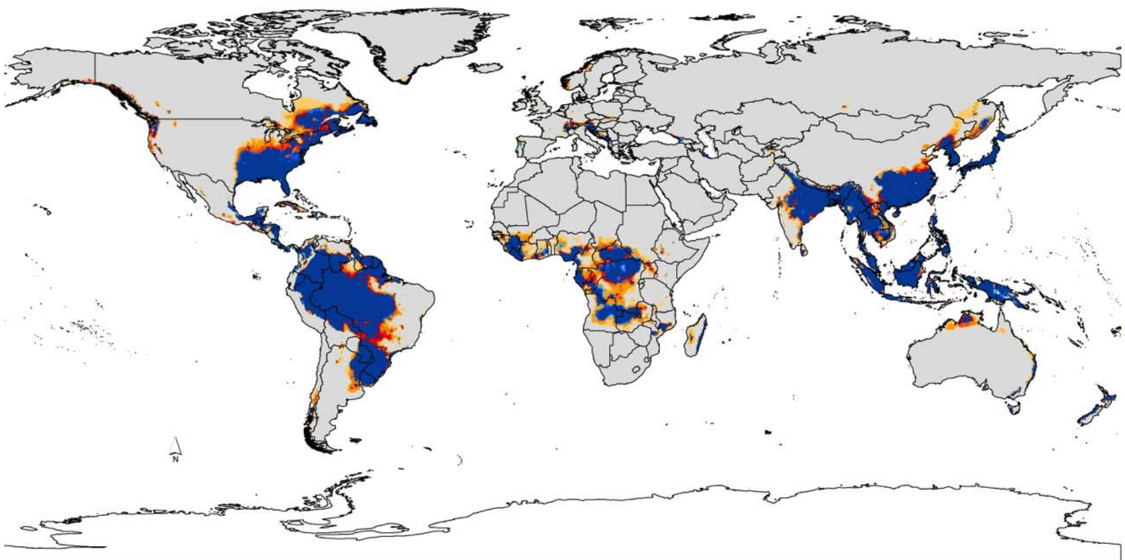

Figure S13. Summary of patterns of co-occurrence derived from ecological niche models of *Aedes aegypti* and *A. albopictus* worldwide, both under current conditions and under modeled future conditions (B1 scenario), based on 8 principal components.

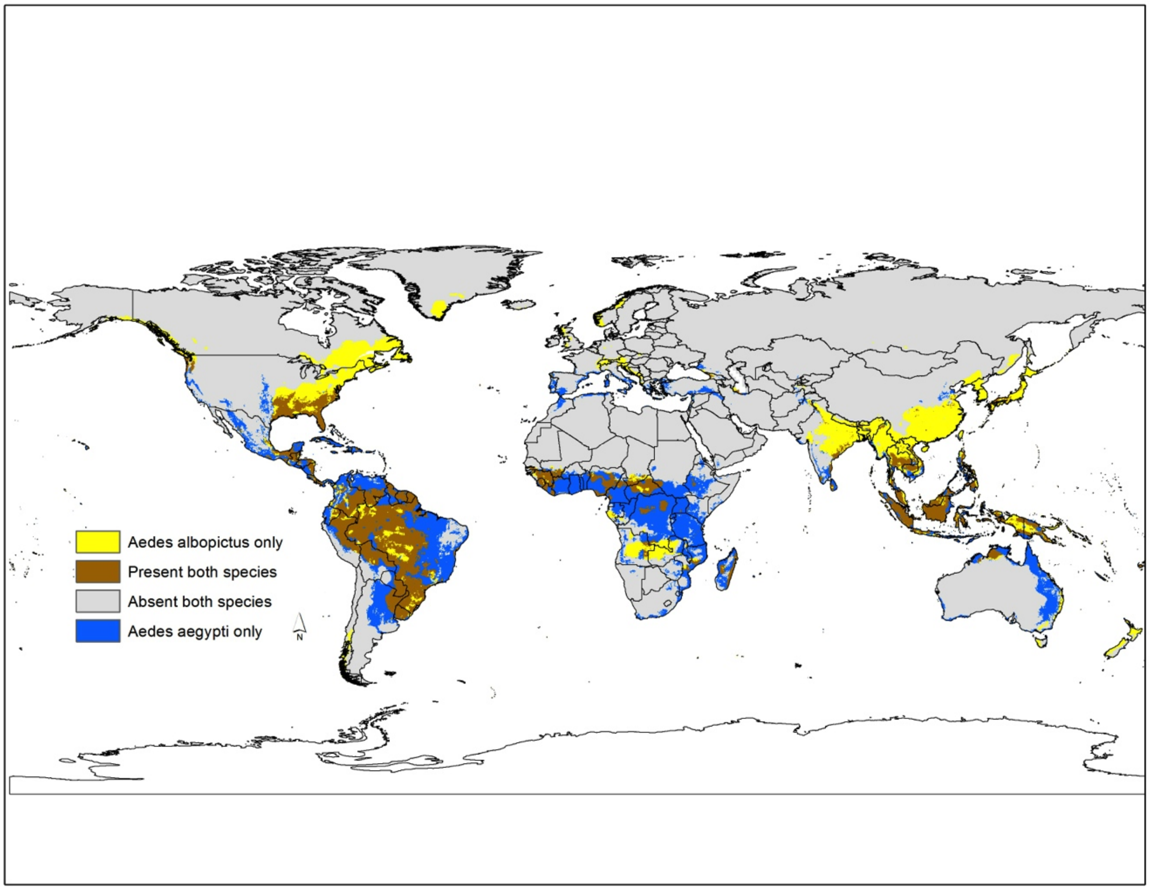

Figure S14. Summary of patterns of co-occurrence derived from ecological niche models of *Aedes aegypti* and *A. albopictus* worldwide, both under current conditions and under modeled future conditions (A2 scenario), based on 8 principal components.

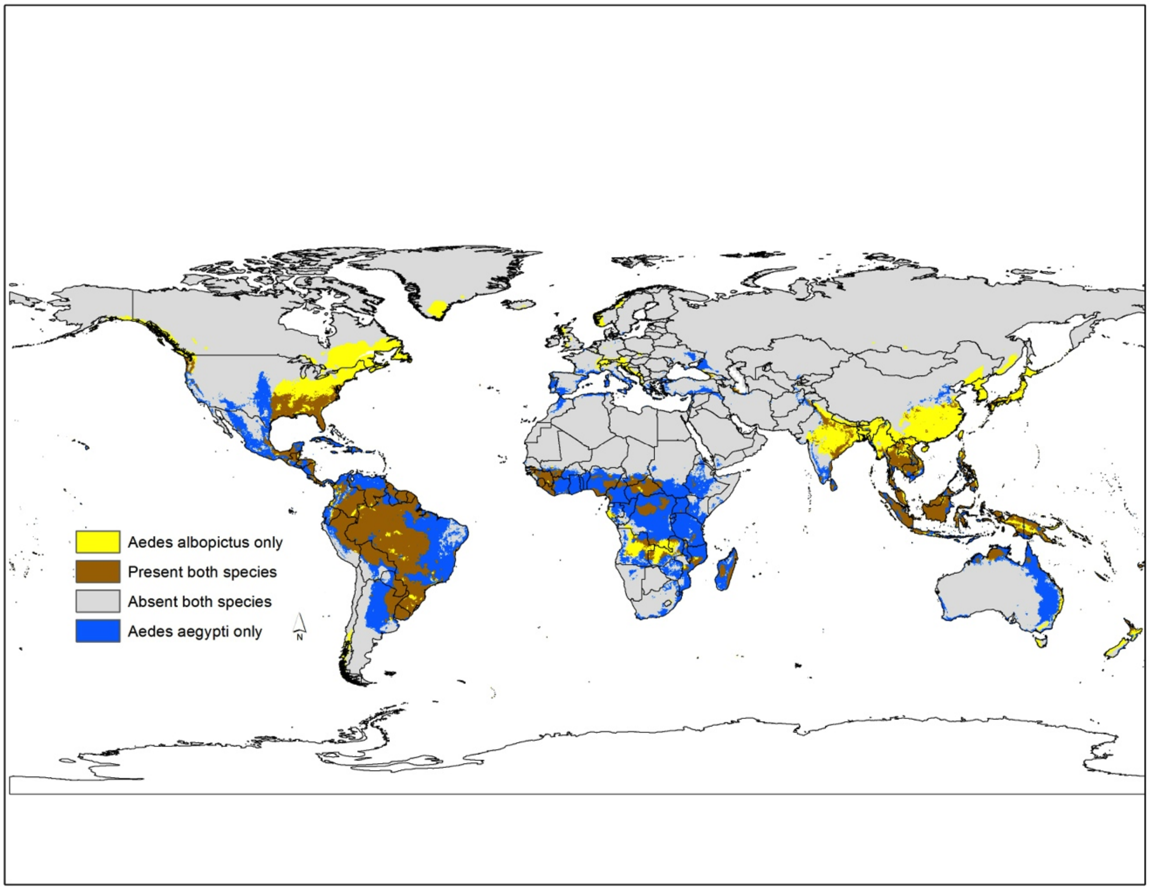

Figure S15. Summary of patterns of co-occurrence derived from ecological niche models of *Aedes aegypti* and *A. albopictus* worldwide, both under current conditions and under modeled future conditions (A1B scenario), based on 6 principal components.

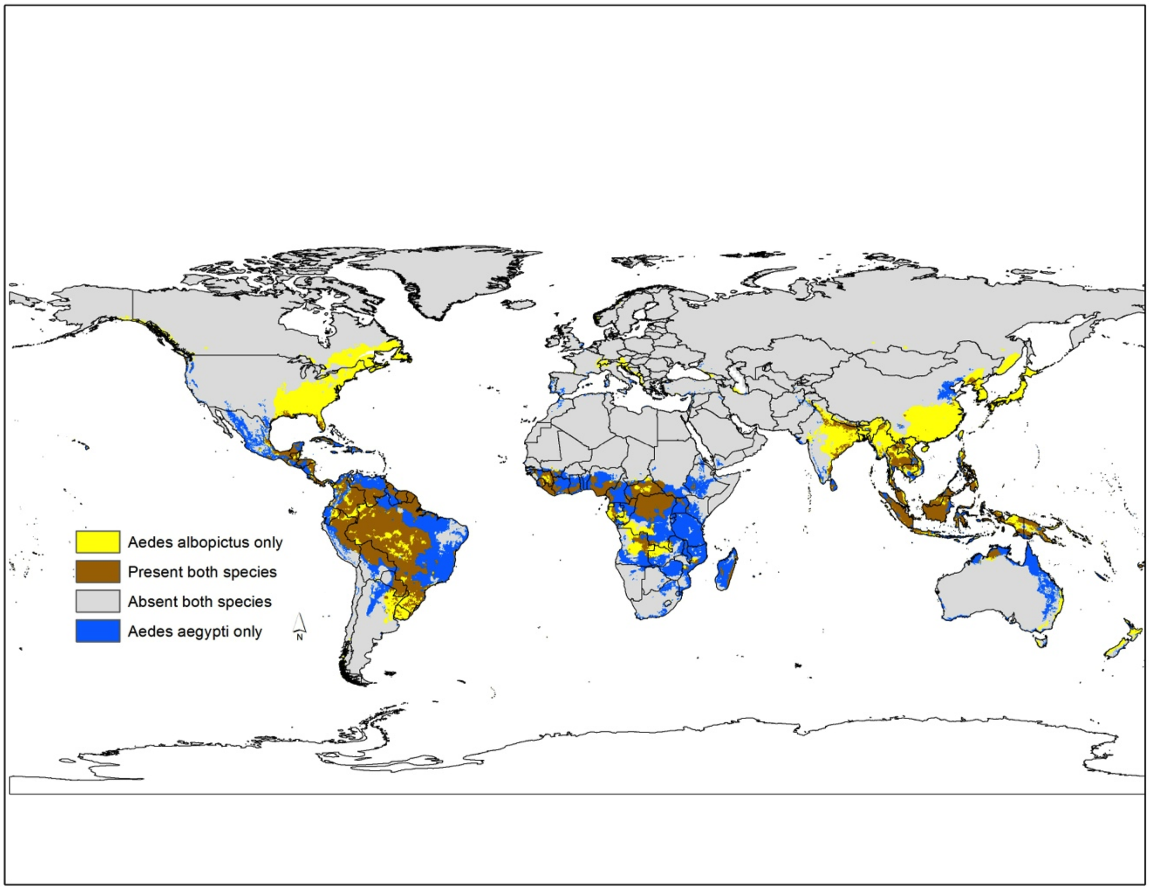

Figure S16. Summary of patterns of co-occurrence derived from ecological niche models of *Aedes aegypti* and *A. albopictus* worldwide, both under current conditions and under modeled future conditions (B1 scenario), based on 6 principal components.

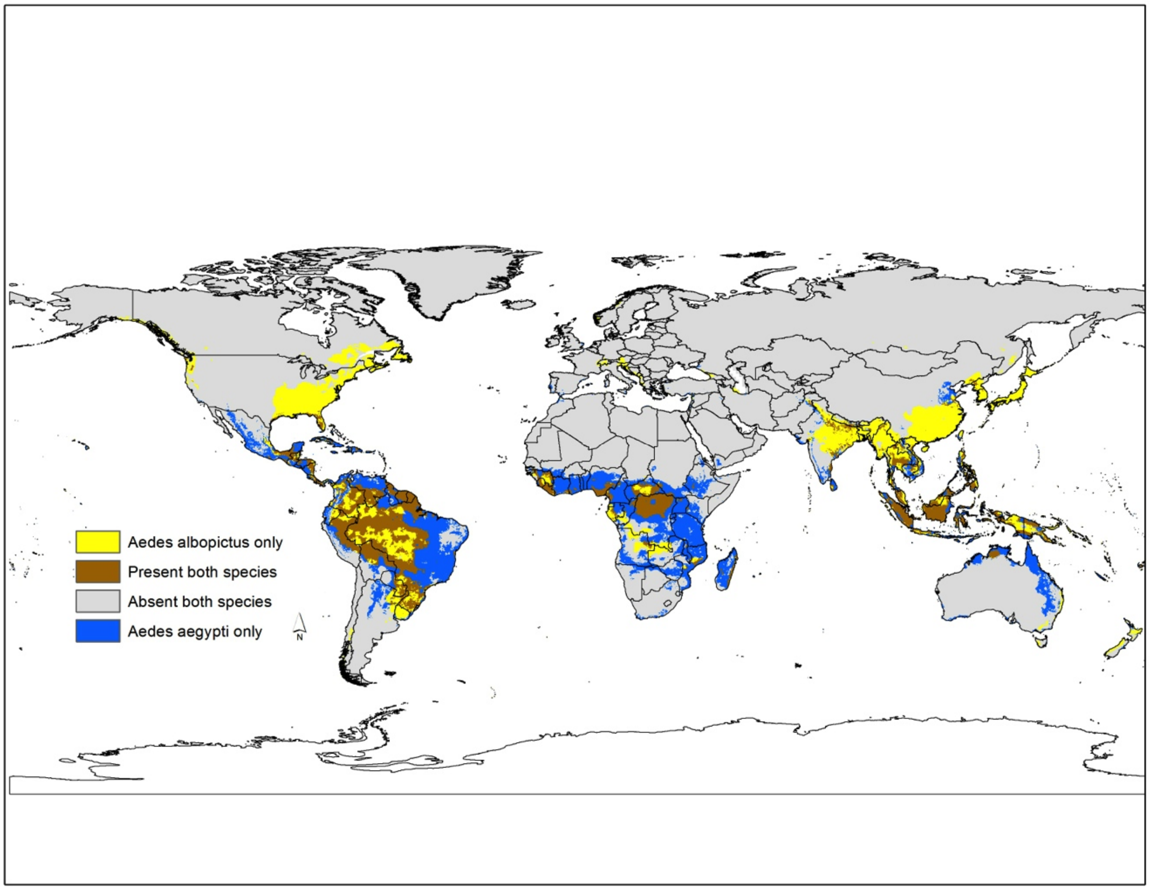

Figure S17. Summary of patterns of co-occurrence derived from ecological niche models of *Aedes aegypti* and *A. albopictus* worldwide, both under current conditions and under modeled future conditions (A2 scenario), based on 6 principal components.

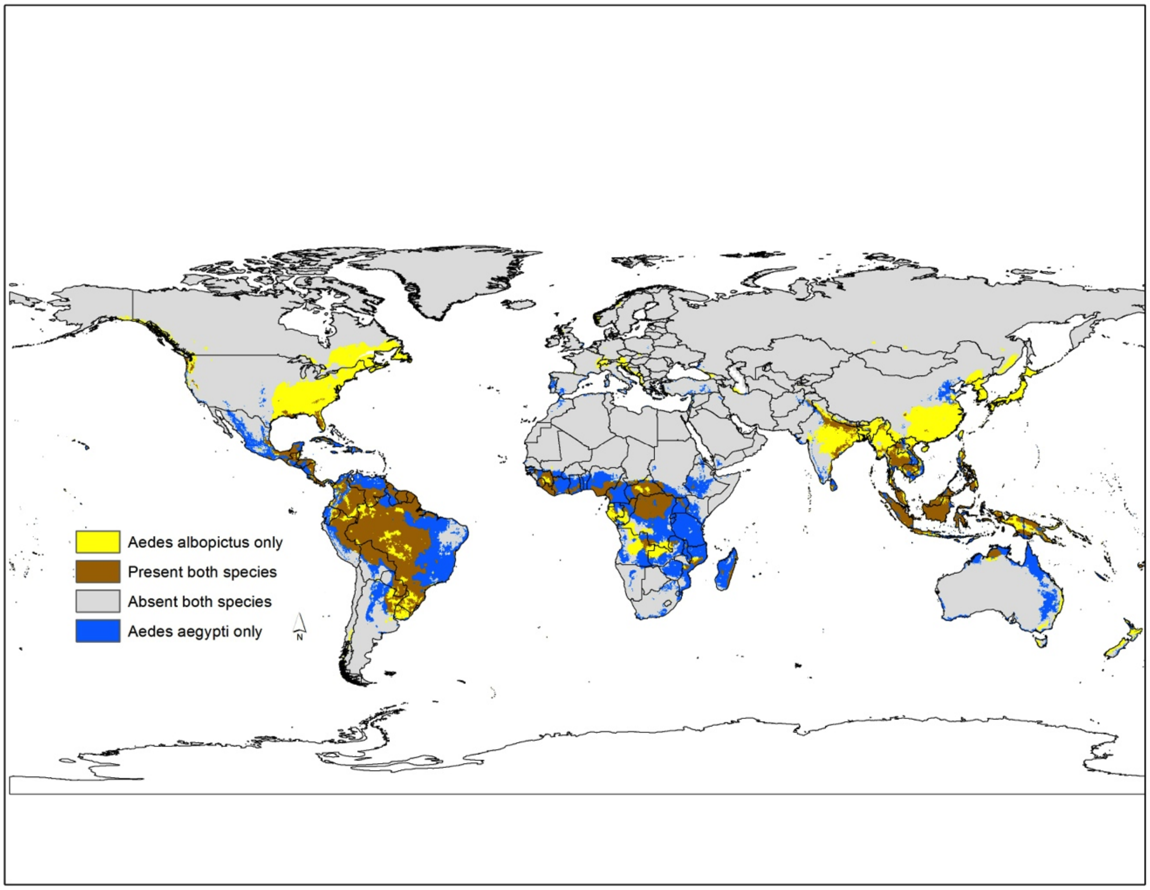

Figure S18. Illustration of the bias surface used to guide sampling of the background in the process of calibration of models in Maxent, with darker blue shades indicating more sampling of *Aedes* mosquitoes from those pixels; gray areas have no sampling. The full dataset is available in GeoTIFF format at http://hdl.handle.net/1808/15275.